ADVANCED FUNCTIONAL MATERIALS
www.afm-journal.de

Nanoparticle Stacks with Graded Refractive Indices Enhance the Omnidirectional Light Harvesting of Solar Cells and the Light Extraction of Light-Emitting Diodes

Cheng-Yi Fang, Yu-Lun Liu, Yang-Chun Lee, Hsuen-Li Chen, De-Hui Wan, and Chen-Chieh Yu*

In this study, nanoparticles (NPs) of various types and sizes are arranged to enhance both the omnidirectional light harvesting of solar cells and the light extraction of light emitting diodes (LEDs). A graded-refractive-index NP stack can minimize reflectance, not only over a broad range of wavelengths but also at different incident angles; the photocurrent of silicon-based solar cells an also be significantly improved omnidirectionally. In addition, the optical gradient of an NP stack can also enhance the light-extraction efficiency of LEDs, due to both the graded refractive index and the moderate surface roughness. Large particles having sizes on the same order of the wavelength of the incident light roughen the LED surfaces further and extract light from beyond the critical angle, as supported by three-dimensional finite-difference time-domain simulations. Using this approach, the photoluminescence intensity can be increased by up to sevenfold. The developed technique: arranging sequences of different NPs in graded-refractive-index stacks, and considering their ability to scatter light due to their sizes and optical constants, may also significantly improve the performance of various optoelectronic devices.

1. Introduction

Nanoparticles (NPs) can enhance the performance of optoelectronic devices because of their convenient fabrication processes and attractive optical properties. Although silicon-based solar cells are the most widely used, the high refractive index of silicon (almost 40% of the incident light is reflected back) means that less light is absorbed and converted to a photocurrent. The major approach toward overcoming this obstacle is minimizing the differences in the refractive indices between the ambient medium and the solar cells. As a result, destructive-interference coatings of antireflective thin films[1,2] have been developed to minimize surface reflection; in addition, several textured structures, including nanoholes,[3] nanowires,[4–6] nanodomes,[7,8] subwavelength gratings,[9] and randomly textured structures[10,11] have been reported. Recently, developments have been made in the coating of NPs onto solar cells without the need for any vacuum systems, etching, or lithography processes, thereby saving time and money. Some of those investigations have focused on increasing absorption through the surface plasmon resonance of metal NPs,[12–15] an approach that we had tested with only a slight enhancement in performance.[16] Others have focused on using ceramic or organic NPs to minimize surface reflection or increase the absorption of the solar cells. The NPs used in those previous studies, including polystyrene (PS), SiC, TiO_2, and SiO_2 spheres, had moderate refractive indices and particle sizes.[15–24] Because the refractive indices of these NPs are all positioned between those of the ambient medium and the solar cells, they could naturally serve in antireflective layers. Some discussions have appeared relating the coupling of light in these particles and the effects of scattering, surface coverage on the solar cells,[17–24] and the effect of particle sizes on absorption.[25] None of them has examined the effects of matching the optical-gradient conditions between the ambient medium and the solar cell. Furthermore, some studies have decreased the average reflectance in the visible and near-infrared (NIR) region to less than 10% through a combination of both etching of the silicon substrate and coating with NPs.[22] According to previous studies, if NPs are used only for scattering or adjusting the surface coverage, NP-based methods will have difficulty competing with the etching of substrates or the construction of multilayer thin-film techniques because of the lack of suitable optical-gradient structures.

Omnidirectional light harvesting is one of the major challenges when designing solar cells. Although some discussions have appeared regarding wide-angle antireflective behavior on silicon-based solar cells, those studies focused on moth-eye or high-aspect-ratio nanostructures[4,6,26,27] prepared using inductively coupled plasma (ICP) etching or oblique sputtering processes. In this paper, we demonstrate that a gradient

C. Y. Fang, Y. L. Liu, Y. C. Lee, Prof. H. L. Chen, Dr. D. H. Wan, C. C. Yu
Department of Materials Science and Engineering
National Taiwan University
Taipei, Taiwan
E-mail: hsuenlichen@ntu.edu.tw

DOI: 10.1002/adfm.201201949

refractive index of NPs can minimize wide-angle reflectance on flat solar cells without the need for any vacuum systems or etching processes that would harm the electrical properties of such solar cells. In contrast to previously reported NP-related research, in this study we used the concept of optical gradients to arrange different types of NPs of various sizes and, thereby, construct NP stacks featuring a gradual change in refractive index, with the goal of improving the broadband and omnidirectional light harvesting of solar cells.

Our aim was to increase the amount light traveling "into" the solar cells devices; in contrast, when dealing with GaN-based light-emitting diodes (LEDs), our aim was to extract light "out of" the devices. Although decreasing the refractive index difference between a GaN substrate and the ambient medium is an important factor, total internal reflection (TIR) and multiple reflections within a limited escape cone make it difficult to improve light extraction. Therefore, roughening the interface between the GaN and the ambient medium is essential to improving light extraction. Many approaches have been developed, including the use of surface texturing,[28–30] photonic crystals,[31] and patterned sapphire substrates, textured ZnO,[32] titanium oxide,[33] or indium-doped tin oxide (ITO) structures[34–37] on GaN-based LEDs. Using NPs to enhance the light-extraction efficiency would, ideally, not require any specific lithography or etching processes, nor expensive vacuum systems. Although TiO_2, ZnO, Al_2O_3, and metallic NPs.[38–43] have all been used previously to increase the light-extraction efficiency of LEDs, all of those previous studies featured only a single type of NP, without any discussions of the effects of the refractive indices of those NPs or their optimal particle sizes. In this study, we coated various types of NP onto LEDs, investigated strategies for arranging different types of NP, and determined the effect of these NPs on the light-extraction efficiency of the LEDs.

For both solar cells and LEDs, coating with NPs can enhance the performance without harming the electrical properties of the devices, as can occur with etching or lithographic processing. Herein, we not only demonstrate this advantageous feature but also provide a strategy for optimizing the types and sizes of NPs for use in both solar cells and LEDs. In addition, we also discuss the omnidirectional light harvesting behavior of solar cells after coating with NPs – a feature that has not been reported from previous NP-based research. Furthermore, we have combined NPs of various sizes and kinds – using a conventional spin-coating method, an economical and rapid process – to enhance the efficiency of light extraction of GaN-based LEDs. We employed different kinds of: i) sub-50 nm-diameter NP to construct an optical gradient NP stack with moderate roughness; and ii) large-sized NPs, as scattering centers that roughened the surface to enhance light extraction. We studied the effects of the different functions and morphologies of both sets of small and large NPs. We then used the three-dimensional finite-difference time-domain (3D-FDTD) method to analyze the optical behavior in the near-field regime of both solar cells and LEDs, with or without the NP stack. Finally, we investigated the optical spectra and device performances. We expect that this strategy of arranging NPs with different materials and sizes could find widespread applicability in various optoelectronic devices.

2. Results and Discussion

In this study, we used several kinds of dielectric NP, which would not absorb in the visible and NIR regimes. Firstly, we investigated the optical behavior of arrays of NPs having sizes of less than 50 nm, arranged in a gradient refractive index profile. As indicated in **Figure 1**a, if the size of each NP in the array and the surface roughness were small relative to the wavelength of incident light, these arrays can be regarded as multilayer optical thin-film stacks with effective refractive indices. Because the surface layer possesses a roughness approximately equal to the particle size (diameter: <50 nm), the degree of scattering of light is low and the system allows the construction of an antireflective layer based on a gradient refractive index for solar cells. We assumed that such multilayer NP arrays behaved as optical thin-film stacks; we then used NPs with different refractive indices to construct a graded-refractive-index profile to enhance both the light harvesting of solar cells and the light extraction of LEDs.

If the sizes of the particles were to be close to the wavelength of incident light, as displayed in Figure 1b, these particles will behave as scattering centers, changing the direction of incident light and roughening the surface. Different optoelectronic devices require different surface morphologies; some need a flat surface to avoid scattering and retain their electrical properties, while others need a moderately rough surface to enhance the light extraction or increase the optical path through a scattering effect. In this study, we prepared both types of system readily through the judicious selection of the nature (types, size) of the NPs and their subsequent spin-coating onto the substrates.

The small-sized dielectric NPs that we coated onto substrates were titanium dioxide (TiO_2), zirconium dioxide (ZrO_2), yttrium oxide (Y_2O_3), aluminum oxide (Al_2O_3), and silicon dioxide

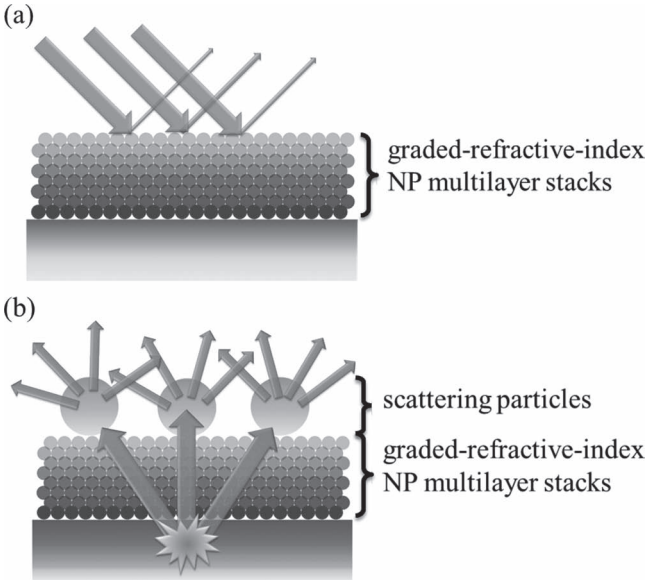

Figure 1. Schematic representation of: a) graded-refractive-index NP multilayer stacks, and b) scattering particles on graded-refractive-index NP stacks.

Table 1. Sizes and effective refractive indices of various NP layers.

	TiO_2	ZrO_2	Y_2O_3	Al_2O_3	SiO_2
Particle size	<15 nm	5–10 nm	20–40 nm	15–20 nm	5–10 nm
Refractive index of bulk material ($\lambda = 600$ nm)	2.49	2.21	1.92	1.76	1.50
Effective refractive index of NP layer ($\lambda = 450$ nm)	1.89	1.57	1.43	1.42	1.21
Effective refractive index of NP layer ($\lambda = 600$ nm)	1.72	1.55	1.41	1.40	1.20

(SiO_2); **Table 1** lists their refractive indices and sizes. Because these NPs are much smaller than the wavelength of visible and NIR light, they would not scatter light to any great degree. We used spin-coating to deposit these NPs onto silicon wafers and then used spectroscopic ellipsometry to determine the effective refractive index. The detailed fitting method has been described elsewhere.[44] Unlike thin films prepared through chemical vapor deposition (CVD) or physical vapor deposition (PVD), NP layers generally possess lower refractive indices than their corresponding bulk materials due to voids between the NPs. The effective refractive indices of these NP layers ranged from 1.89 to 1.20 (Table 1).

Conventionally, the optical thickness of a destructive-interference-based antireflection coating on a solar cell should be equal to one quarter of the specific wavelength; this method can eliminate the reflectance at a specific wavelength, leaving the reflectance high in the other wavelength regions. To ensure broadband antireflection properties, the antireflective coating must feature a graded refractive index; here, we used different NP layers to readily form such a structure. Moreover, because bulk materials featuring a refractive index near 1.20 do not exist, low-refractive-index optical thin films have been prepared previously through oblique-angle deposition.[5,45] In this study, positioning low-refractive-index layers (e.g., SiO_2 NPs) on top of gradient-refractive-index NP stacks allowed us to achieve broadband antireflection layers. Therefore, this rapid, low-cost, solution-based method allows the construction of graded-refractive-index NP stacks that function as broadband, omnidirectional antireflection coatings.

We used the 3D-FDTD method to analyze the optical behavior of light propagating within the near-field regime on the surfaces of silicon substrates. **Figure 2** displays the behavior of a plane wave propagating from 400 nm above the air/antireflection-structure interface to the silicon surface in the absence and presence of graded-refractive-index NPs. Figure 2a presents the reflection behavior of plane waves having wavelengths of 500, 650, and 800 nm incident to bare silicon substrates. The reflectance values collected by the detectors from left to right in Figure 2a were 39.5%, 35.4%, and 33.4%, respectively. Figure 2b presents the behavior

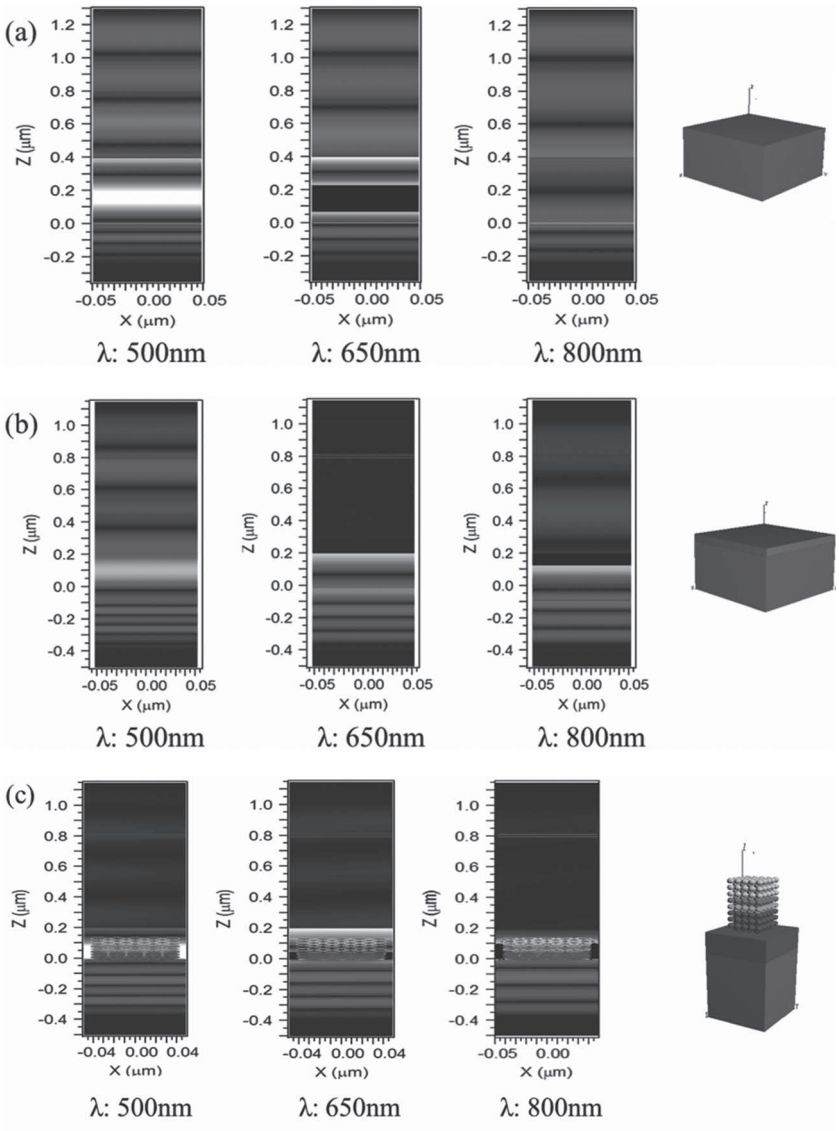

Figure 2. Plane waves propagating from 400 nm above the air-Si interface to: a) bare Si, b) 80 nm Si_3N_4 on Si, and c) a graded-refractive-index NP stack on Si (incident light at wavelengths of 500, 650, and 800 nm, from left to right).

of a plane wave having the same wavelengths on silicon featuring a Si_3N_4 film – that is, a conventional single-layer antireflective coating (SLARC) that would decrease the reflective light at a specific wavelength, and the calculated reflectance values of plane waves having wavelengths of 500, 650, and 800 nm were 12%, 0.8%, and 4.5%, respectively. The surface reflectance in Figure 2a is significant; in Figure 2b, the conventional single-layer antireflective coating largely eliminates the reflective light at a wavelength of 650 nm, but significant reflectance remained at other wavelengths. Figure 2c presents the behavior of plane waves propagating toward a graded-refractive-index NP stack on 60 nm TiO_2-thin-film-coated silicon substrate. The sequence of this NP stack, from the top of the TiO_2 thin film to the air, was TiO_2, ZrO_2, Al_2O_3, and SiO_2 NPs. Noticeably, the reflectance did not decrease at only a single wavelength, but rather within a broad range of wavelength. The reflectance values collected by the detectors in Figure 2c were 2.2%, 0.9%, and 1.3%, respectively.

Next, we experimentally investigated the antireflective behavior of a graded-refractive-index NP stack, which we prepared through spinning of TiO_2, ZrO_2, Al_2O_3, and SiO_2 NPs sequentially onto a planar silicon substrate. Table 1 provides detailed parameters for these NPs. **Figure 3**a displays a cross-sectional scanning electron microscopy (SEM) image of this graded-refractive-index NP stack; its structure was not well ordered because the sizes of the particles were not monodisperse. The surface was not sufficiently rough to scatter light significantly, as we will demonstrate below. The large-scale view in the inset to Figure 3a reveals that the surface is quite flat.

Figure 3b presents the reflectance spectra of the optical gradient NP stack, measured using a spectrometer equipped with an integrating sphere to ensure that all of the reflective light was counted. The reflectance of a flat silicon wafer coated with the graded-refractive-index NP stack was significantly lower (circles) compared with that of the flat silicon wafer (squares). The average reflectance decreased from 35.71% to 10.61%, which is lower than the silicon nitride-based SLARC deposited through plasma-enhanced chemical vapor deposition (PECVD).[46] Nevertheless, to decrease the reflectance at different surfaces, the refractive index difference between each layer should be diminished. The effective refractive indices of our NP layers were in the range from 1.89 to 1.20; this range is too low to construct a good antireflective stack on a silicon substrate (n = 3.4 at a wavelength of 600 nm). Thus, we firstly deposited a TiO_2 layer having a thickness of 100 nm onto the silicon wafer; the refractive index of this TiO_2 thin film was 2.20 at a wavelength of 600 nm. Next, we spun the NPs onto the TIO_2 thin film in the same sequence as before to form a graded refractive index. As

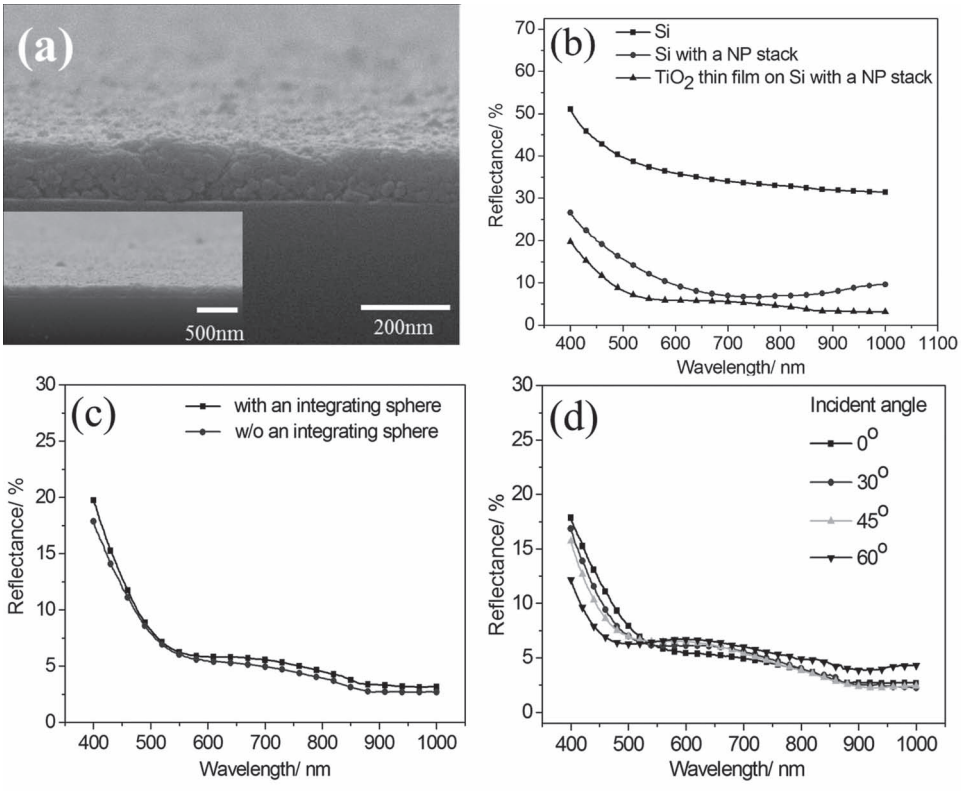

Figure 3. a) SEM image of a graded-refractive-index NP stack on Si (TiO_2, ZrO_2, Al_2O_3, and SiO_2 NPs in sequence from the Si wafer to the air). b) Reflectance spectra of Si (squares), Si with a graded-refractive-index NP multilayer stack (circles), and a TiO_2 thin film on Si with a graded-refractive-index NP multilayer stack (triangles). c) Reflectance spectra, recorded with an integrating sphere (squares) and without an integrating sphere (circles), of a sputtered TiO_2 thin film on Si in the absence of an NP stack. d) Reflectance spectra of a sputtered TiO_2 thin film on Si in the presence of a graded-refractive-index NP multilayer stack, recorded at different incident angles.

displayed in Figure 3b, the reflectance (triangles) was lower than those of the other two surfaces over a broad range of wavelengths; the average reflectance (6.26%) was lower than that of a previously reported silicon nitride/MgF_2 double-layer antireflective coating (DLARC).[46]

To determine the effect of the surface morphology in Figure 3a, we measured the reflectance spectra of this sample using a spectrometer with and without an integrating sphere. Without the integrating sphere, the spectrometer measured light only at a reflective angle equal to the incident angle (i.e., specular reflection); with the integrating sphere, the spectrometer recorded the reflectance of all the light scattered by the NP structure. Conventional measurements of reflectance without the use of an integrating sphere will count only the specular reflectance and preclude the detection of scattered light, which can lead to a misreading of the real optical behavior if the surface is not smooth. If the reflectance measured using the integrating sphere was almost the same as that measured without the integrating sphere, the scattered intensity would be small, indicating a smooth surface with respect to the scale of the wavelength of the incident light. As displayed in Figure 3c, the difference between the measured reflectance with and without the use of the integrating sphere was less than 1%, suggesting that almost all of the light traveled along the same direction as the incident light. This behavior is similar to that of multilayer optical thin films. Moreover, the graded-refractive-index NP stack was also effective at decreasing the reflectance at large incident angles. Figure 3d presents the reflectance spectra measured at different incident angles using non-polarized light. When the incident angle was 60°, the average reflectance was less than 8%, comparable with the values found for broadband and omnidirectional antireflection structures prepared using complicated techniques.[26,27,47] Therefore, without using an etching process, we could rapidly and cheaply fabricate low-reflectance broadband and omnidirectional antireflection surfaces.

We deposited a graded-refractive-index NP stack atop a planar silicon solar cell to induce an increased photocurrent in the device. **Figure 4**a displays the photocurrent response of the planar silicon solar cell before and after spin-coating of the graded-refractive-index NP stack, normalized with respect to the photocurrent response of the corresponding cell in the absence of the graded-refractive-index NP stack. These spectra were recorded under unpolarized illumination at normal incident angle. The cell coated with the graded-refractive-index NP stack exhibited an enhancement (by ca. 40%) in photocurrent over the entire wavelength region. Figure 4b presents the photocurrent response of the solar cell measured at an incident angle of 60°. The solar cell coated with the graded-refractive-index NP stack exhibited an enhancement in photocurrent (by ca. 60%) over the entire wavelength region, with the increase in photocurrent reaching over 80% in the short-wavelength regime. Furthermore, Figure 4c displays the relationship between the normalized photocurrent and the incident angle at a wavelength of 660 nm (the photocurrents are normalized to that of a flat silicon solar cell without the coating of the graded-refractive-index NP stack, under illumination at normal incidence). Because the surface reflection increased dramatically upon increasing the incident angle, the photocurrent of the silicon solar cells would

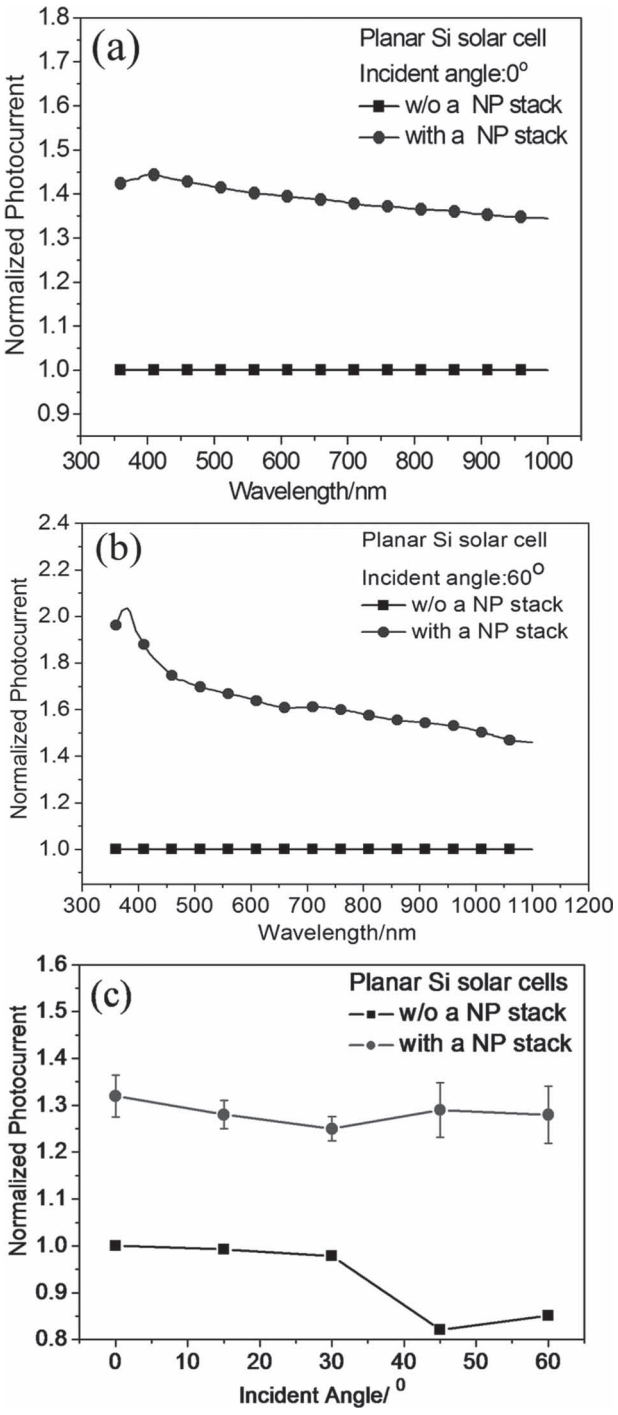

Figure 4. Normalized photocurrent spectra of the graded-refractive-index NP multilayer stack coated on a planar Si cell, measured under non-polarized illumination at incident angles of: a) 0° and b) 60° (multilayers of TiO_2, ZrO_2, Al_2O_3, and SiO_2 NPs from the top of the cells to the air). c) Photocurrents recorded at different incident angles at a wavelength of 660 nm.

decrease significantly. After coating with the graded-refractive-index NP stack, the photocurrents under illumination at large incident angles were almost the same as that at normal incident angle, consistent with the reflectance spectrum in Figure 3d.

In the previous study, the solar cell coated with a single SiO_2 nanoparticle layer exhibited a limited enhancement of ca. 8% at an incident angle of 60°[48] due to the lack of a gradient refractive index, compared with that of the solar cell coated with graded-refractive-index NP stack (about ca. 60%). Thus, the graded-refractive-index NP stack could decrease the reflectance even at large incident angles. To the best of our knowledge, this enhancement in omnidirectional photocurrent is much greater than those obtained in previous reports of metal or dielectric NP-enhanced solar cells.[15,22,49]

Because the main issue in this study was how to manipulate the refractive index profiles at different interfaces, for such an NP stack to be applied to other optoelectronic devices, it would have to have a variable-refractive-index profile. As displayed in **Figure 5**a, we examined the relatively complex issue of light extraction from GaN-based multiple-quantum-well (MQW) LEDs. The high refractive index of GaN ($n = 2.5$) prohibits light beyond a critical angle of 23.5° from being extracted according to the conditions of TIR. A rough surface is generally required to enhance the escape probability of photons generated in the active layer of an LED. Moreover, the Fresnel reflectance at the GaN-air interface is approximately 18%, meaning that even if the light were not beyond the critical angle, 18% of the light generated in the active layer would be reflected back into the device. Therefore, we constructed a graded-refractive-index NP stack on the GaN surface to prevent light from reflecting back into the active layer. Because the top layer of the LED was ITO, we investigated the optical properties at the ITO-air interface. The high transparency and low sheet resistance make ITO films good transparent electrodes. In this study, we found that the graded-refractive-index NP stack also served as an antireflective layer on the ITO surface, increasing the transmittance without harming the underlying electrical properties. Figure 5b displays the measured transmission spectra of an ITO film coated on a glass substrate before and after coating with the graded-refractive-index NP stack. The sequence of NPs that we deposited is this case, from ITO to the air, was Y_2O_3, Al_2O_3, and SiO_2. Because the refractive index of ITO is 1.88 at 600 nm, we did not have to deposit a film with as high a refractive index as we did on the silicon substrate. As displayed in Figures 5b,c, the transmittance in the visible and NIR regions increased after adding the graded-refractive-index NP stack, while retaining the sheet resistance at 10 Ω per □, because the spin-coating process did not change the structure of the ITO glass. This NP-coated transparent electrode with higher transmittance could presumably be used on various optical devices – not only LEDs but also organic light emitting diodes (OLEDs) and organic solar cells. Furthermore, as displayed in Figure 5c, the graded refractive index decreased the reflectance of the ITO-air interface, meaning that once the light had arrived at the ITO layer from the LED it would travel through the graded-refractive-index NP stack with less loss than through the ITO-air interface directly. We implemented this property to enhance the light-extraction efficiency of LEDs.

We spin-coated ZrO_2, Y_2O_3, Al_2O_3, and SiO_2 NP multilayers in sequence on top of an LED device. This graded-refractive-index NP stack decreased the Fresnel reflection strongly at the GaN-ITO-air interfaces. Indeed, light within the escape cone experienced virtually no Fresnel reflection. Moreover, due to the slight roughness of these NP thin films, they also served to slightly suppress TIR. Next, we deposited larger particles, with sizes close to the wavelength of incident light, to further roughen the surface. These larger particles, SiO_2 NPs having a

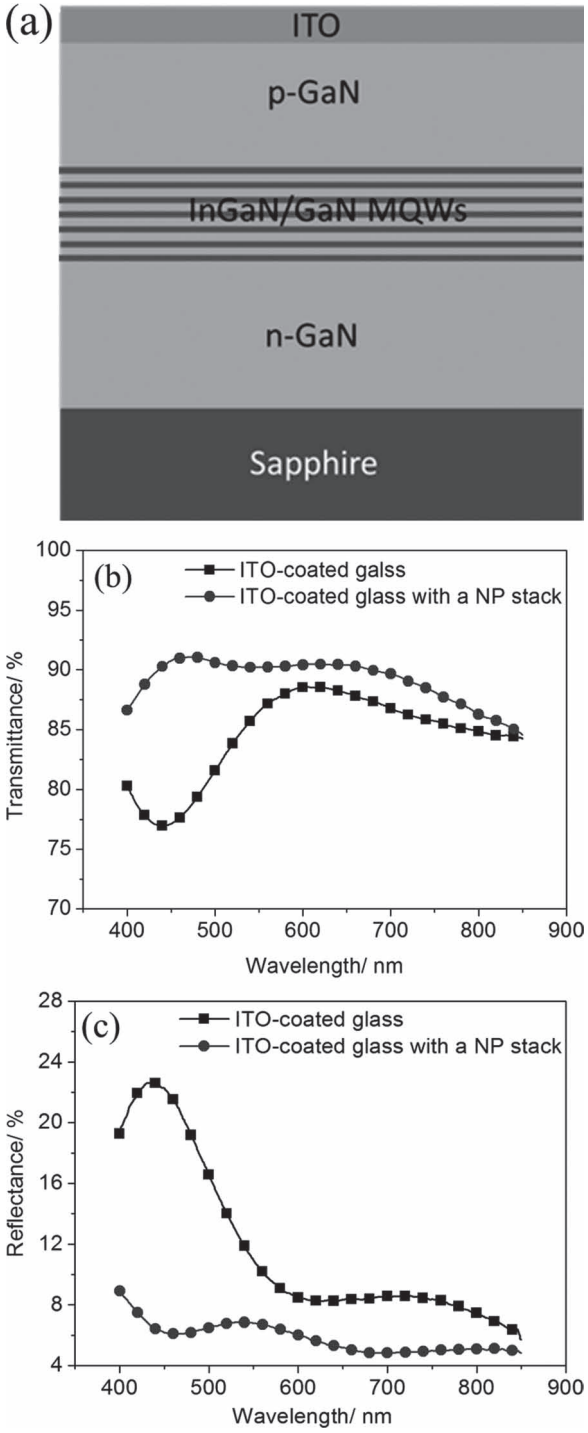

Figure 5. a) Schematic representation of a GaN/InGaN-based LED. b,c) Transmittance (b) and reflectance (c) spectra of ITO-coated glass in the absence (squares) and presence (circles) of a graded-refractive-index NP multilayer stack (multilayers of Y_2O_3, Al_2O_3, and SiO_2 NPs from the top of the ITO to the air).

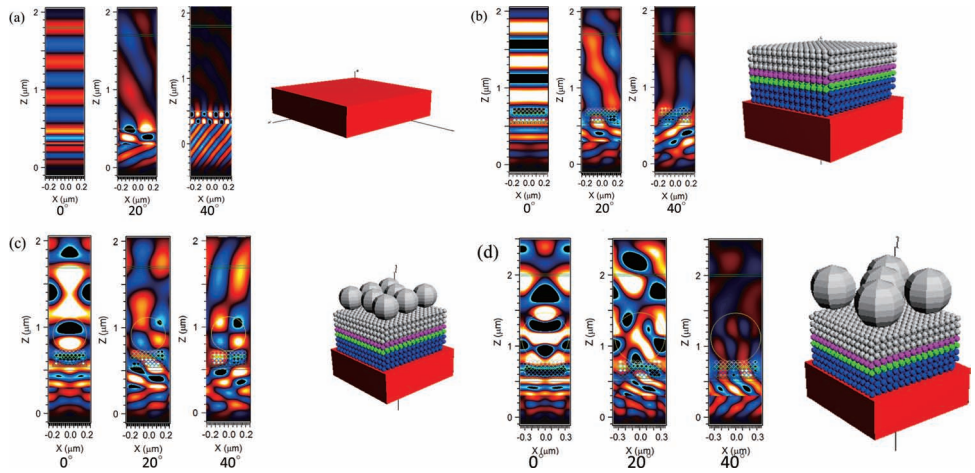

Figure 6. Plane waves propagated from 200 nm under the air-GaN interface to: a) bare GaN, b) a graded-refractive-index NP multilayer stack (each 40 nm in diameter) and 60 nm ITO on GaN, c) SiO_2 particles (diameter: 460 nm) on the same structure as in (b), and d) SiO_2 particles (diameter: 1000 nm) on the same structure as in (b); incident angles of 0, 20, and 40°, from left to right.

diameter of 460 nm, behaved as scattering centers. As displayed in Figure 1b, we proposed to firstly use the graded-refractive-index NP stack to extract light from the ITO-air interface and then use the larger scattering particles to change the optical behavior of the flat surface to enhance the light-extraction efficiency of the LEDs.

We applied the 3D-FDTD method to simulate the optical behavior of a plane wave under and above GaN-air and GaN-NP interfaces (**Figure 6**). We set the wavelength of 450 nm, to model the wavelength of light emitted from GaN-based LEDs. Figure 6a displays the optical behavior of bare GaN with light source located 200 nm beneath the GaN-air interface, with incident angles of 0, 20, and 40°. The extraction efficiency decreased upon increasing the incident angle of light under the GaN-air interface. Moreover, light at an incident angle larger than the critical angle (23.5°) could not be extracted. Next, we placed a graded-refractive-index NP stack on the ITO/GaN surface. The sequence of the NPs in the stack, from top of the ITO film to the air, was ZrO_2, Y_2O_3, Al_2O_3, and SiO_2; each particle size was 40 nm – less than one tenth of the wavelength of light generated by the GaN-based LEDs (ca. 450 nm). Figure 6b displays the simulated optical behavior of extracted light launched at incident angles of 0, 20, and 40°. The presence of the graded-refractive-index NP stack enhanced the light output significantly within the critical angle (23.5°). When the incident angle was 40° (i.e., beyond the critical angle), only a small amount of light was extracted out, presumably because the surface of the NP layer was slightly rough and, therefore, suppressed TIR. Because the NPs were much smaller than the wavelength of incident light, however, we observed only a slight degree of scattering. Notably, the roughness can be neglected when dealing with antireflective behavior on the solar cells; when dealing with the suppression of TIR, however, the surface morphology must play an important role. As displayed in Figure 6b, when the incident angle was 40°, our sub-50 nm NPs provided only a slightly disrupted flat surface. Therefore, we had to use larger SiO_2 scattering particles to roughen the surface further. In Figure 6c, we placed much larger SiO_2 particles (diameter: 460 nm) on top of the graded-refractive-index NP stack to function as scattering centers. The incident angles in this 3D-FDTD simulation were also 0, 20, and 40°. Notably, when the light was incident beyond the critical angle, the light extracted from the surface was enhanced significantly. We suspect that when the light arrived at this surface, the graded-refractive-index stack constructed from small dielectric NPs (diameter: <50 nm) caused it to pass through with little reflection loss; when the light being extracted propagated to the top of the graded-refractive-index NP stack, the larger SiO_2 scattering particles (diameter: 460 nm – close to the wavelength of the incident light) provided a rougher surface that largely suppressed TIR. Therefore, large amounts of light could be extracted from the GaN-based LED surface. We found that 460 nm SiO_2 particles provided an excellent amount of scattered light. If the size of the SiO_2 particles was to increase to the micrometer scale, we believe that the light-extraction efficiency would decrease because the light would follow the traditional rules of geometrical optics, with some of the extracted light refracting or reflecting back to the surface of the GaN-based LEDs. This phenomenon is evident in Figure 6d, where the graded-refractive-index NP stack is the same as that in Figure 6c, except for the larger size of the top-most scattering SiO_2 particles – 1000 nm, much larger than the wavelength of incident light. Beyond the critical angle, less light was extracted than that in Figure 6c. We conclude that, to enhance to the light-extraction efficiency, it is necessary to choose scattering particles having a size approximating the wavelength of that light.

Next, we experimentally investigated the light-extraction phenomena of the InGaN/GaN MQW LEDs. Here, we spin-coated a graded-refractive-index NP stack comprising, in sequence, ZrO_2, Y_2O_3, Al_2O_3, and SiO_2 NPs; Table 1 lists the refractive indices and sizes. Finally, we spin-coated 460 nm SiO_2 scattering particles on top of the graded-refractive-index NP stack. **Figure 7**a displays an SEM image of these scattering particles, which were closely packed and covered most of the surface. Figure 7b presents an enlarged SEM image, revealing the much smaller graded-refractive-index NPs beneath the large scattering SiO_2 particles.

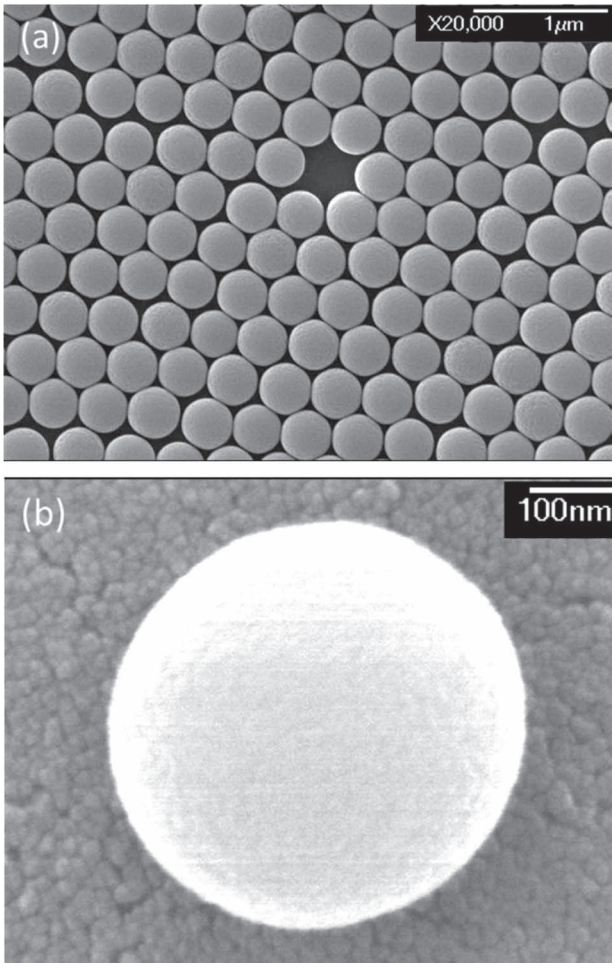

Figure 7. SEM images of: a) 460 nm SiO_2 particles and b) graded-refractive-index NPs beneath a large SiO_2 particle.

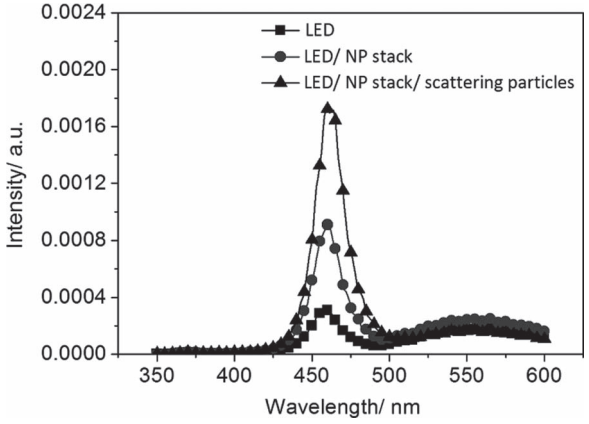

Figure 8. PL spectra, measured at room temperature, of the reference LED (squares), the LED coated with a graded-refractive-index NP multilayer stack (circles), and the LED coated with a graded-refractive-index NP multilayer stack and scattering 460 nm SiO_2 particles (triangles).

To verify the light-extraction enhancement of LEDs, we measured photoluminescence (PL) spectra of InGaN/GaN LED samples, with and without the NP coating, at room temperature using a 325 nm He-Cd laser (**Figure 8**). The peak wavelength of the PL spectra appeared near 460 nm. The PL intensity of the LED coated with the graded-refractive-index NP stack (circles) was up to three times higher than that of the reference LED sample (squares). This behavior arose from both the antireflective behavior and the moderate roughness presented by the optical-gradient NPs. After spin-coating large SiO_2 scattering particles (diameter: 460 nm), the PL intensity (triangles) increased to seven times higher than that of the reference LED sample (squares). Obviously, the large SiO_2 particles served as scattering centers that roughened the surface further and, therefore, suppressed TIR dramatically. The enhancement in light-extraction efficiency that we achieved through the use of spin-coating procedures in this study is comparable with or better than those achieved previously using patterned surfaces,[50–52] other NPs[44,53] or surface-plasmon-related studies.[54] Because we did not use any etching processes, our method will not harm the electrical properties of the underlying devices. We can reasonably suppose that the degrees of enhancement of the PL intensities will be similar when applied in real LED chips. Moreover, spin-coating processes are simple, rapid, and inexpensive, and they do not require the use of vacuum systems, lithography, or chemical etchants. Therefore, this strategy for arranging NPs saves processing time and money while improving the light-extraction efficiencies of LEDs and the omnidirectional light harvesting of solar cells.

3. Conclusions

In this study, we have developed a strategy for arranging dielectric NPs of various types and sizes to enhance both the omnidirectional light harvesting of solar cells and the light extraction of LEDs. We investigated the optical behavior and performance on silicon solar cells and GaN/InGaN-based LEDs after coating graded-refractive-index NP stacks and scattering particles onto these devices. We used an optical spectrometer to measure the amount of scattered light, 3D-FDTD simulations to determine the near-field behavior, and SEM to observe the surface structures. To enhance the omnidirectional antireflection behavior of solar cells, we used sub-50 nm NPs (i.e., with sizes less than one tenth of the wavelength of incident light) to construct graded-refractive-index layers, which decreased the reflectance not only within a broad wavelength region but also at different incident angles. Furthermore, the photocurrents of the silicon solar cells were improved significantly at different incident angles. In addition, these sub-50 nm NPs also improved the light-extraction efficiency of GaN/InGaN-based LEDs, due to their graded refractive indices and moderate surface roughness. Larger particles having sizes on the same order of the incident wavelength roughened the surface further to extract a greater amount of light beyond the critical angle. 3D-FDTD simulations supported these findings. Using this approach, the PL intensity could be enhancement by up to seven times. Therefore, our technique of arranging sequences of different particles into graded-refractive-index stacks, taking advantage of their ability to scatter light because of their sizes and optical constants, appears to have great potential for improving the

performance of various optoelectronic devices. Because our fabrication approach involves rapid and simple spin-coating and does not require any etching, the electrical properties of the devices will remain unimpaired. The underlying strategy is to match the optical constants while considering the effects of scattering under different wavelengths. This NP-related technique appears to have great potential for application to other optoelectronic devices, including thin-film solar cells, organic solar cells, transparent conductors, and OLEDs.

4. Experimental Section

Materials: All of the chemicals were used as received. The titanium oxide colloid solution in xylene (TiO_2, 45–47%) featured particles having diameters of less than 15 nm. The zirconium dioxide colloid solution in water (ZrO_2, 10%) contained particles having diameters of approximately 5–10 nm. The yttrium(III) oxide colloid solution in isopropyl alcohol (Y_2O_3, 10%) featured particles having an average diameter of 20–40 nm. The aluminum oxide colloid solution in water (Al_2O_3, 10%) contained particles having an average diameter of approximately 15–20 nm. The colloidal solution of the smaller silicon dioxide NPs in water (SiO_2, 10%) featured particles having diameters of approximately 5–10 nm; that of the larger silicon dioxide NPs (SiO_2, 5%) contained particles having diameters of approximately 460 nm.

Graded-Refractive-Index NP Stacks on Solar Cells: The TiO_2 solution (diluted to 4 wt% with isopropyl alcohol) was spun onto cleaned silicon substrates before heating at 100 °C for 10 min. After cooling to room temperature, the ZrO_2 solution (diluted to 2 wt% with isopropyl alcohol and water), Al_2O_3 solution (diluted to 1 wt% with EtOH), and the SiO_2 solution (diluted to 3 wt% with isopropyl alcohol and water) were spun onto the surfaces in sequence. For some of the samples mentioned in the article, 100 nm-thick TiO_2 films were grown on the Si substrates through sputtering. Ar and O_2 (1:10) were supplied at a pressure of 1.8×10^{-3} Torr.

Graded-Refractive-Index NP Stacks and Scattering NPs on LEDs: These samples were obtained using the approach described above, but with the ZrO_2 solution (diluted to 2 wt% with isopropyl alcohol and water), Y_2O_3 solution (diluted to 4 wt% with isopropyl alcohol), Al_2O_3 solution (diluted to 2 wt% with EtOH), the smaller SiO_2 solution (diluted to 3 wt% with isopropyl alcohol and water), and the larger SiO_2 (460 nm) solution (diluted to 4 wt% with isopropyl alcohol and water) spun onto the surfaces in sequence.

Simulation and Characterization: The 3D-FDTD method was used to analyze the optical behavior in the near-field regime of the graded-refractive-index NP stacks deposited on silicon substrates and the graded-refractive-index NP stacks presenting large scattering particles on GaN LEDs. The reflectance spectra were measured using a Hitachi U4100 optical spectrometer. The substrates featuring deposited NPs were observed using a JEOL JSM-6500F scanning electron microscope. The photocurrent spectra of these devices were obtained using a Xe lamp as the illumination source and a grating monochromator having a grating of 1200 grooves per mm, yielding the light source with a bandwidth of ca. 10 nm for measurements scanning over the detection wavelength range 350–1100 nm and a Keithley 2400 semiconductor parameter analyzer.

Acknowledgements

We thank the National Science Council, Taiwan, for supporting this study under contracts NSC-100-2628-E-002-031-MY3 and NSC-100-2623-E-002-003-ET.

Received: July 13, 2012
Revised: September 18, 2012
Published online: October 16, 2012

[1] H. Nagel, A. G. Aberle, R. Hezel, *Prog. Photovoltiacs* **1999**, *7*, 245.
[2] S. H. Lee, I. Lee, J. Yi, *Surf. Coat. Technol.* **2002**, *153*, 67.
[3] K. Q. Peng, X. Wang, L. Li, X. L. Wu, S. T. Lee, *J. Am. Chem. Soc.* **2010**, *132*, 6872.
[4] M. D. Kelzenberg, S. W. Boettcher, J. A. Petykiewicz, D. B. Turner-Evans, M. C. Putnam, E. L. Warren, J. M. Spurgeon, R. M. Briggs, N. S. Lewis, H. A. Atwater, *Nat. Mater.* **2010**, *9*, 239.
[5] J. Q. Xi, J. K. Kim, E. F. Schubert, *Nano Lett.* **2005**, *5*, 1385.
[6] K. Q. Peng, S. T. Lee, *Adv. Mater.* **2011**, *23*, 198.
[7] J. Zhu, C. M. Hsu, Z. F. Yu, S. H. Fan, Y. Cui, *Nano Lett.* **2010**, *10*, 1979.
[8] Y. L. Li, H. Y. Yu, J. S. Li, S. M. Wong, X. W. Sun, X. L. Li, C. W. Cheng, H. J. Fan, J. Wang, N. Singh, P. G. Q. Lo, D. L. Kwong, *Small* **2011**, *7*, 3138.
[9] J. W. Leem, Y. M. Song, Y. T. Lee, J. S. Yu, *Appl. Phys. B: Lasers Opt.* **2010**, *100*, 891.
[10] D. H. Wan, H. L. Chen, S. Y. Chuang, C. C. Yu, Y. C. Lee, *J. Phys. Chem. C* **2008**, *112*, 20567.
[11] S. C. Tseng, H. L. Chen, C. C. Yu, Y. S. Lai, H. W. Liu, *Energy Environ. Sci.* **2011**, *4*, 5020.
[12] K. L. Kelly, E. Coronado, L. L. Zhao, G. C. Schatz, *J. Phys. Chem. B* **2003**, *107*, 668.
[13] D. M. Schaadt, B. Feng, E. T. Yu, *Appl. Phys. Lett.* **2005**, *86*, 063106.
[14] S. Pillai, K. R. Catchpole, T. Trupke, M. A. Green, *J. Appl. Phys.* **2007**, *101*, 093105.
[15] S. P. Sundararaian, N. K. Grady, N. Mirin, N. J. Halas, *Nano Lett.* **2008**, *8*, 624.
[16] D. H. Wan, H. L. Chen, T. C. Tseng, C. Y. Fang, Y. S. Lai, F. Y. Yeh, *Adv. Funct. Mater.* **2010**, *20*, 3064.
[17] T. H. Chang, P. H. Wu, H. Chen, C. H. Chan, C. C. Lee, C. C. Chen, Y. K. Su, *Opt. Express* **2009**, *17*, 6519.
[18] Y. A. Akimov, W. S. Koh, S. Y. Sian, S. Ren, *Appl. Phys. Lett.* **2010**, *96*, 073111.
[19] B. G. Lee, P. Stradins, D. L. Young, K. Alberi, T. K. Chuang, J. G. Couillard, H. M. Branz, *Appl. Phys. Lett.* **2011**, *99*, 064101.
[20] Y. Wang, L. Chen, H. Yang, Q. Guo, W. Zhou, M. Tao, *Sol. Energy Mater. Sol. Cells* **2009**, *93*, 85.
[21] D. Derkacs, W. V. Chen, P. M. Matheu, S. H. Lim, P. K. L. Yu, E. T. Yu, *Appl. Phys. Lett.* **2008**, *93*, 091107.
[22] C. K. Huang, H. H. Lin, J. Y. Chen, K. W. Sun, W. L. Chang, *Sol. Energy Mater. Sol. Cells* **2011**, *95*, 2540.
[23] J. Grandidier, D. M. Callahan, J. N. Munday, H. A. Atwater, *Adv. Mater.* **2011**, *23*, 1272.
[24] S. Nunomura, A. Minowa, H. Sai, M. Kondo, *Appl. Phys. Lett.* **2010**, *97*, 063507.
[25] J. Grandidier, M. Deceglie, D. Callahan, H. Atwater, *J. Photonics Energy* **2012**, *2*, 024502.
[26] B. D. Park, J. W. Leem, J. S. Yu, *Appl. Phys. B: Lasers Opt.* **2011**, *105*, 335.
[27] Y. P. Chen, H. C. Chiu, G. Y. Chen, C. H. Chiang, C. T. Tseng, C. H. Lee, L. A. Wang, *Microelectron. Eng.* **2010**, *87*, 1323.
[28] E. Trichas, M. Kayambaki, E. Iliopoulos, N. T. Pelekanos, P. G. Savvidis, *Appl. Phys. Lett.* **2009**, *94*, 173505.
[29] T. Fujii, Y. Gao, R. Sharma, E. L. Hu, S. P. DenBaars, S. Nakamura, *Appl. Phys. Lett.* **2004**, *84*, 855.
[30] D. W. Kim, H. Y. Lee, M. C. Yoo, G. Y. Yeom, *Appl. Phys. Lett.* **2005**, *86*, 052108.
[31] D. H. Kim, C. O. Cho, Y. G. Roh, H. Jeon, Y. S. Park, J. Cho, J. S. Im, C. Sone, Y. Park, W. J. Choi, Q. H. Park, *Appl. Phys. Lett.* **2005**, *87*, 203508.
[32] C. Battaglia, J. Escarre, K. Soderstrom, M. Charriere, M. Despeisse, F. J. Haug, C. Ballif, *Nat. Photonics* **2011**, *5*, 535.
[33] J. Grandidier, D. Callahan, J. Munday, H. Atwater, *IEEE J. Photovoltaics* **2012**, *2*, 123.

[34] K. H. Dai, C. B. Soh, S. J. Chua, L. S. Wang, D. X. Huang, *J. Appl. Phys.* **2011**, *109*, 083110.
[35] K. S. Kim, S. M. Kim, H. Jeong, M. S. Jeong, G. Y. Jung, *Adv. Funct. Mater.* **2010**, *20*, 1076.
[36] D. S. Liu, T. W. Lin, B. W. Huang, F. S. Juang, P. H. Lei, C. Z. Hu, *Appl. Phys. Lett.* **2009**, *94*, 143502.
[37] J. K. Kim, S. Chhajed, M. F. Schubert, E. F. Schubert, A. J. Fischer, M. H. Crawford, J. Cho, H. Kim, C. Sone, *Adv. Mater.* **2008**, *20*, 801.
[38] F. W. Mont, J. K. Kim, M. F. Schubert, E. F. Schubert, R. W. Siegel, *J. Appl. Phys.* **2008**, *103*, 083120.
[39] P. Uthirakumar, B. D. Ryu, J. H. Kang, H. G. Kim, J. H. Ryu, C. H. Hong, *Vacuum* **2010**, *85*, 198.
[40] B. D. Ryu, P. Uthirakumar, J. H. Kang, B. J. Kwon, S. Chandramohan, H. K. Kim, H. Y. Kim, J. H. Ryu, H. G. Kim, C. H. Hong, *J. Appl. Phys.* **2011**, *109*, 093116.
[41] T. K. Kim, S. H. Kim, S. S. Yang, J. K. Son, K. H. Lee, Y. G. Hong, K. H. Shim, J. W. Yang, K. Y. Lim, S. J. Bae, G. M. Yang, *Appl. Phys. Lett.* **2009**, *94*, 161107.
[42] J. H. Sung, J. S. Yang, B. S. Kim, C. H. Choi, M. W. Lee, S. G. Lee, S. G. Park, E. H. Lee, B. H. O, *Appl. Phys. Lett.* **2010**, *96*, 261105.
[43] C. Y. Cho, K. S. Kim, S. J. Lee, M. K. Kwon, H. Ko, S. T. Kim, G. Y. Jung, S. J. Park, *Appl. Phys. Lett.* **2011**, *99*, 041107.
[44] D. H. Wan, H. L. Chen, Y. S. Lin, S. Y. Chuang, J. Shieh, S. H. Chen, *ACS Nano* **2009**, *3*, 960.
[45] J. Q. Xi, M. F. Schubert, J. K. Kim, E. F. Schubert, M. F. Chen, S. Y. Lin, W. Liu, J. A. Smart, *Nat. Photonics* **2007**, *1*, 176.
[46] K. C. Sahoo, M. K. Lin, E. Y. Chang, Y. Y. Lu, C. C. Chen, J. H. Huang, C. W. Chang, *Nanoscale Res. Lett.* **2009**, *4*, 680.
[47] J. W. Leem, J. S. Yu, *Thin Solid Films* **2011**, *519*, 3792.
[48] X. Lu, Z. Wang, X. Yang, X. Xu, L. Zhang, N. Zhao, J. Xu, *Surf. Coat. Technol.* **2011**, *206*, 1490.
[49] C. Hagglund, M. Zach, G. Petersson, B. Kasemo, *Appl. Phys. Lett.* **2008**, *92*, 053110.
[50] E. J. Hong, K. J. Byeon, H. Park, J. Hwang, H. Lee, K. Choi, H. S. Kim, *Solid-State Electron.* **2009**, *53*, 1099.
[51] E. J. Hong, K. J. Byeon, H. Park, J. Hwang, H. Lee, K. Choi, G. Y. Jung, *Mater. Sci. Eng., B* **2009**, *163*, 170.
[52] M. Park, G. Yu, K. Shin, *Cryst. Growth* **2011**, *326*, 28.
[53] B. J. Kim, J. Bang, S. H. Kim, J. Kim, *J. Electrochem. Soc.* **2010**, *157*, H449.
[54] K. Okamoto, I. Niki, A. Shvartser, Y. Narukawa, T. Mukai, A. Scherer, *Nat. Mater.* **2004**, *3*, 601.